MOFBOTS: Metal–Organic-Framework-Based Biomedical Microrobots

Xiaopu Wang, Xiang-Zhong Chen, Carlos C. J. Alcântara, Semih Sevim, Marcus Hoop, Anastasia Terzopoulou, Carmela de Marco, Chengzhi Hu, Andrew J. de Mello, Paolo Falcaro, Shuhei Furukawa, Bradley J. Nelson, Josep Puigmartí-Luis,* and Salvador Pané

Motile metal–organic frameworks (MOFs) are potential candidates to serve as small-scale robotic platforms for applications in environmental remediation, targeted drug delivery, or nanosurgery. Here, magnetic helical microstructures coated with a kind of zinc-based MOF, zeolitic imidazole framework-8 (ZIF-8), with biocompatibility characteristics and pH-responsive features, are successfully fabricated. Moreover, it is shown that this highly integrated multifunctional device can swim along predesigned tracks under the control of weak rotational magnetic fields. The proposed systems can achieve single-cell targeting in a cell culture media and a controlled delivery of cargo payloads inside a complex microfluidic channel network. This new approach toward the fabrication of integrated multifunctional systems will open new avenues in soft microrobotics beyond current applications.

Wireless micro- and nanorobots are tiny devices that have the ability to swim in different liquid environments powered by either chemical fuels spread in their surroundings, or by means of external energy sources, such as magnetic fields, electric fields, ultrasound, light, or combinations of these.[1] These small-scale devices have been used for many applications, particularly in the biomedical field.[2] With the ability to convey therapeutic agents or cells to difficult-to-reach sites of the human body, micro- and nanorobots have the potential to revolutionize many areas of medicine. Progress in this research field is fundamentally linked to advances in materials science and micro- and nanomanufacturing.[1d,3] While many recently developed materials are suitable candidates as components in micro- and nanorobotic platforms, their assimilation into a highly integrated multifunctional device has been an ongoing challenge.[1f]

Currently, interest is focused on providing locomotion to soft structures with high porosity and tunable physicochemical properties, such as metal–organic frameworks (MOFs), because of their potential applications as controllable microcarriers.[4] While initial efforts have been made to produce mobile MOF-based small-scale machines,[4a,5] the locomotion features of most of these systems lack the level of sophistication of current state-of-the-art micro- and nanoswimmers. For example, the controlled directionality of chemically propelled MOF crystals has yet to be addressed.[6] In contrast, while magnetically driven MOFs can be guided using an external magnetic field, their locomotion mechanism is mainly limited to magnetic dragging, which requires high magnetic field gradients.[7]

Here, we present a helical MOF-based micromachine that can swim and follow complex trajectories under the control of weak rotational magnetic fields. We focused our research on zeolitic imidazole framework-8 (ZIF-8) due to its excellent biocompatibility and degradation characteristics in relatively mild acidic conditions.[8] We also show that our highly integrated multifunctional micromachine can successfully release drugs to a designated location, where the pH values are around 6, which corresponds to the similar acidic conditions found in tumor microenvironments.[9] This integrated micromachine is tumor responsive, it enables selectively automated drug delivery and its motion can be precisely controlled, giving it an advantage over previous drug delivery platforms, which have only achieved one of these key features.[10]

In the fabrication process, two-photon polymerization (2PP) stereolithography was used to generate 3D structures on which

X. Wang, Dr. X.-Z. Chen, C. C. J. Alcântara, Dr. M. Hoop, A. Terzopoulou, Dr. C. de Marco, Dr. C. Hu,[+] Prof. B. J. Nelson, Dr. S. Pané
Institute of Robotics and Intelligent Systems
ETH Zurich
Tannenstrasse 3, CH-8092 Zurich, Switzerland
S. Sevim, Prof. A. J. de Mello, Dr. J. Puigmartí-Luis
Institute for Chemical and Bioengineering
ETH Zurich
Tannenstrasse 3, CH-8092 Zurich, Switzerland
E-mail: josep.puigmarti@chem.ethz.ch
Prof. P. Falcaro
Institute of Physical and Theoretical Chemistry
Graz University of Technology
Stremayrgasse 9, 8010 Graz, Austria
Prof. P. Falcaro
Department of Chemistry
The University of Adelaide
Adelaide, South Australia 5005, Australia
Prof. S. Furukawa
Institute for Integrated Cell-Material Sciences (WPI-iCeMS)
Kyoto University
Yoshida, Sakyo-ku, Kyoto 606-8501, Japan

(iD) The ORCID identification number(s) for the author(s) of this article can be found under https://doi.org/10.1002/adma.201901592.

[+]Present address: Department of Mechanical and Energy Engineering, Southern University of Science and Technology, No 1088 xueyuan Blvd. Xili, 518055 Shenzhen, China
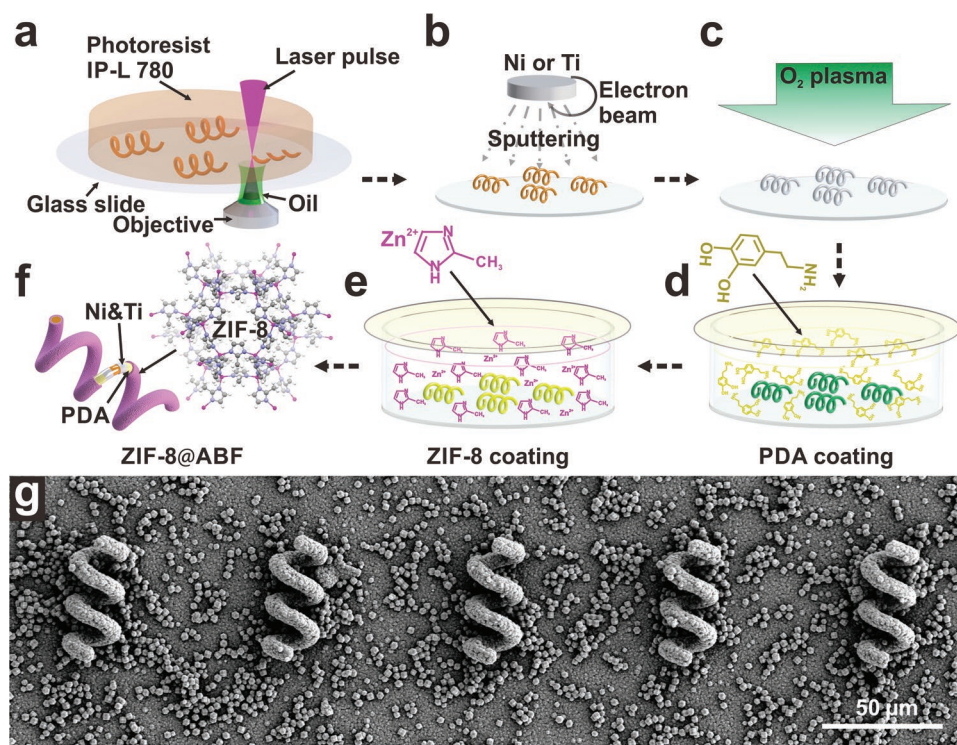
Figure 1. a–f) Schematic illustration of the component steps involved in the manufacture of ZIF-8@ABF microrobots, detailed explanations can be found in the main text. g) An SEM image of multiple ZIF-8@ABFs.

MOF crystals were grown through a seeded bottom-up synthesis. We fabricated helical swimmers, also known as artificial bacterial flagella (ABF) with 2PP (**Figure 1**a) and coated them with nickel and then titanium (Figure 1b) to make them magnetic and biocompatible. Next, the sample was treated with O_2 plasma (Figure 1c) to help the growth of polydopamine (PDA) on the ABF surface (Figure 1d). After functionalization with PDA, MOF crystals were grown on the ABF surface (Figure 1e), as heterogeneous nucleation driven by PDA promotes MOF growth.[11] We focused our investigations on the growth of ZIF-8, because of its exceptional thermal and chemical stability in water media and its pH-responsive features.[12] We used different concentrations and reaction times to ensure a complete coating of PDA functionalized ABFs with ZIF-8, called ZIF-8@ABFs from now on (Figure 1f). Figure 1g shows an SEM image of multiple ZIF-8@ABFs.

As shown in **Figure 2**a, we found that a compact and homogeneous coating with ZIF-8 was achieved by immersing PDA functionalized ABFs in a methanolic solution of $Zn(NO_3)_2$ (25×10^{-3} M) and 2-methylimidazole (50×10^{-3} M) for a period of 24 h. Comparison of ZIF-8 fabricated with different reactant concentrations and reacting times is shown in the supporting information and Figure S1 (Supporting Information). As clearly observed by scanning electron microscopy (SEM), maintaining the same concentrations of reactant but with a reduced reaction time of 2 h resulted in an undesirable partial coating of the ABF surface (Figure S1, Supporting Information). Additionally, under this condition, the synthesized ZIF-8 crystals were not uniform in size, varying between 150 and 450 nm. Conversely, increasing reactant concentrations (i.e., $Zn(NO_3)_2$ 50×10^{-3} M and 2-methylimidazole 100×10^{-3} M) while maintaining a reaction time of

24 h, rendered ZIF-8@ABFs with rough surfaces unsuitable for smooth maneuvering of the composite structures in solution (Figure S1a-VI, Supporting Information); this could be caused by an overgrowth of ZIF-8 on ABFs. A decrease in reactant concentrations (i.e., $Zn(NO_3)_2$ 10×10^{-3} M and 2-methylimidazole 20×10^{-3} M) resulted in a considerable number of pristine (unmodified) ABF structures, and these conditions were not considered further in our investigation (see Supporting Information and Figure S2 in the same for further details). Note that in all these experiments, the ratio of zinc nitrate over 2-methylimidazole concentrations was kept constant at a value of 0.5.

After the ZIF-8 coating optimization, ZIF-8@ABFs were characterized using energy dispersive X-ray analysis (EDS) and X-ray diffraction (XRD) studies, to unambiguously confirm the elemental composition and crystalline nature of the MOF structure. EDS analysis with SEM revealed the presence of Zn, N, and C throughout the ZIF-8@ABF structures, indicating their compact and homogeneous coating with ZIF-8 crystals (Figure 2b). In addition, the XRD plot obtained from the powder of the ZIF-8 coating was almost identical to the pattern reported in the literature for ZIF-8 crystals (see Figure S2 in the Supporting Information).[13] These results confirm the sodalite crystalline nature of the ZIF-8 coating on PDA functionalized ABFs.

The swimming behavior of ZIF-8@ABF structures was investigated in water by applying an alternative rotational magnetic field (generated by Helmholtz coils) to a suspension of ZIF-8@ABFs. The relationship between the forward speed of ZIF-8@ABFs and the rotating frequency of the magnetic field at 4 mT is shown in Figure 2c. Three different swimming conditions were clearly identified: i) wobbling motion below 10 Hz,
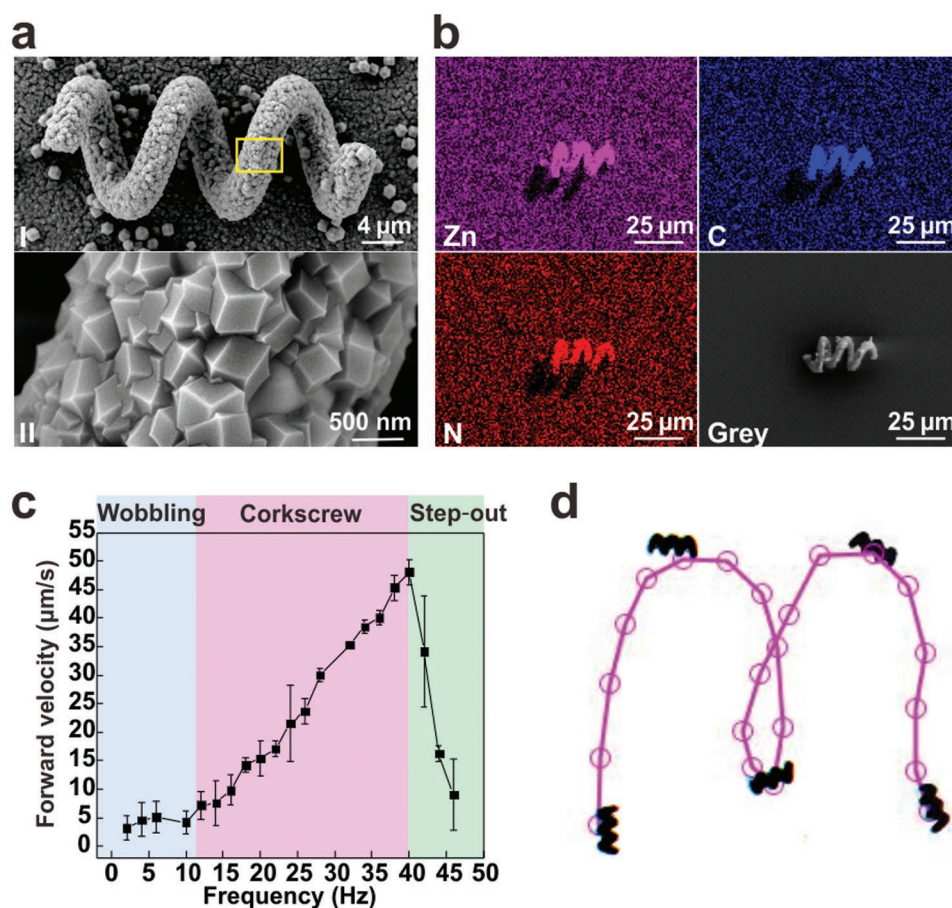
ADVANCED
SCIENCE NEWS
www.advancedsciencenews.com

ADVANCED
MATERIALS
www.advmat.de

Figure 2. a-i) SEM image of ZIF-8@ABFs fabricated after 24 h in a methanolic solution of $Zn(NO_3)_2$ (25×10^{-3} M) and 2-methylimidazole (50×10^{-3} M), and ii) an enlarged SEM image of the area marked by the yellow box in (i). b) SEM-EDX images of a ZIF-8@ABF structure. c) Variation of the forward velocity as a function of frequency for ZIF-8@ABFs when applying a rotational magnetic field of 4 mT. Each point corresponds to the average speed of three ZIF-8@ABF microrobots ($n = 3$). d) Trajectory of a ZIF-8@ABF microrobot following a predesigned track.

ii) corkscrew motion between 10 and 40 Hz, and iii) step-out condition above 40 Hz. Generally, by increasing the frequency of the rotating magnetic field, the propulsion speed of the helical swimmer increases until the step-out frequency is reached. Note that the step-out frequency is the maximum frequency by which a magnetic swimmer can rotate synchronously with the applied magnetic field. Above this frequency the magnetic body rotates asynchronously. In other words, the swimmer cannot follow the rotating magnetic field, and consequently its propulsion speed decreases as the frequency increases. By changing the direction and the rotating frequency of the magnetic field, the ZIF-8@ABF can be navigated along a user-designed path. Figure 2d shows the trajectory of a ZIF-8@ABF tracking a predesigned pattern "m." Video S1 reports the trajectory of a ZIF-8@ABF writing the letters "mof." This controlled motion can also be extended to a third dimension as shown in Video S2. These results demonstrate that the mobility and location of ZIF-8@ABFs can be precisely remotely controlled.

SEM investigations revealed that the integrity of ZIF-8@ABFs was maintained even when the structures were kept for 24 h in a phosphate buffer solution (PBS) at pH 7.4 (**Figure 3**a). However, as shown in Figure 3a, ZIF-8 crystals on ZIF-8@ABFs were significantly degraded after being exposed to a

slightly acidic PBS solution (pH 6.0) for a period of 12 h. It has been reported that mildly acidic conditions can prompt the degradation of ZIF-8 crystals,[8] which makes this material ideal for drug delivery applications in cancer therapy, as cancer cells are typically surrounded by a different environment than that of normal cells. Note that changes or gradients in pH in body fluids have been a source of inspiration for the development of several pH-responsive micro- and nanoswimmers.[14] The extracellular medium in cancerous tissues has been shown to exhibit a slightly acidic pH, with values ranging from 5 to 6.[9] Accordingly, the pH dependent stability of ZIF-8 on ZIF-8@ABFs provides an unprecedented system (the mobile 3D MOF structure) that behaves as a pH-responsive microrobot for targeted drug delivery applications.

To confirm the potential of ZIF-8@ABFs as drug carrier microrobots, we loaded fluorescent rhodamine B (RhB) as a drug model compound to the ZIF-8 crystals of ZIF-8@ABFs, hereafter referred to as RhB@ZIF-8@ABFs. The encapsulation of RhB in ZIF-8 was carried out following a one-pot protocol, as described in the literature, but with some minor modifications.[8c] RhB@ZIF-8@ABFs were fabricated by immersing PDA functionalized ABFs in a methanolic solution of $Zn(NO_3)_2$ (25×10^{-3} M), 2-methylimidazole (50×10^{-3} M) and RhB (1×10^{-3} M) for 24 h.

**ADVANCED
SCIENCE NEWS**

www.advancedsciencenews.com
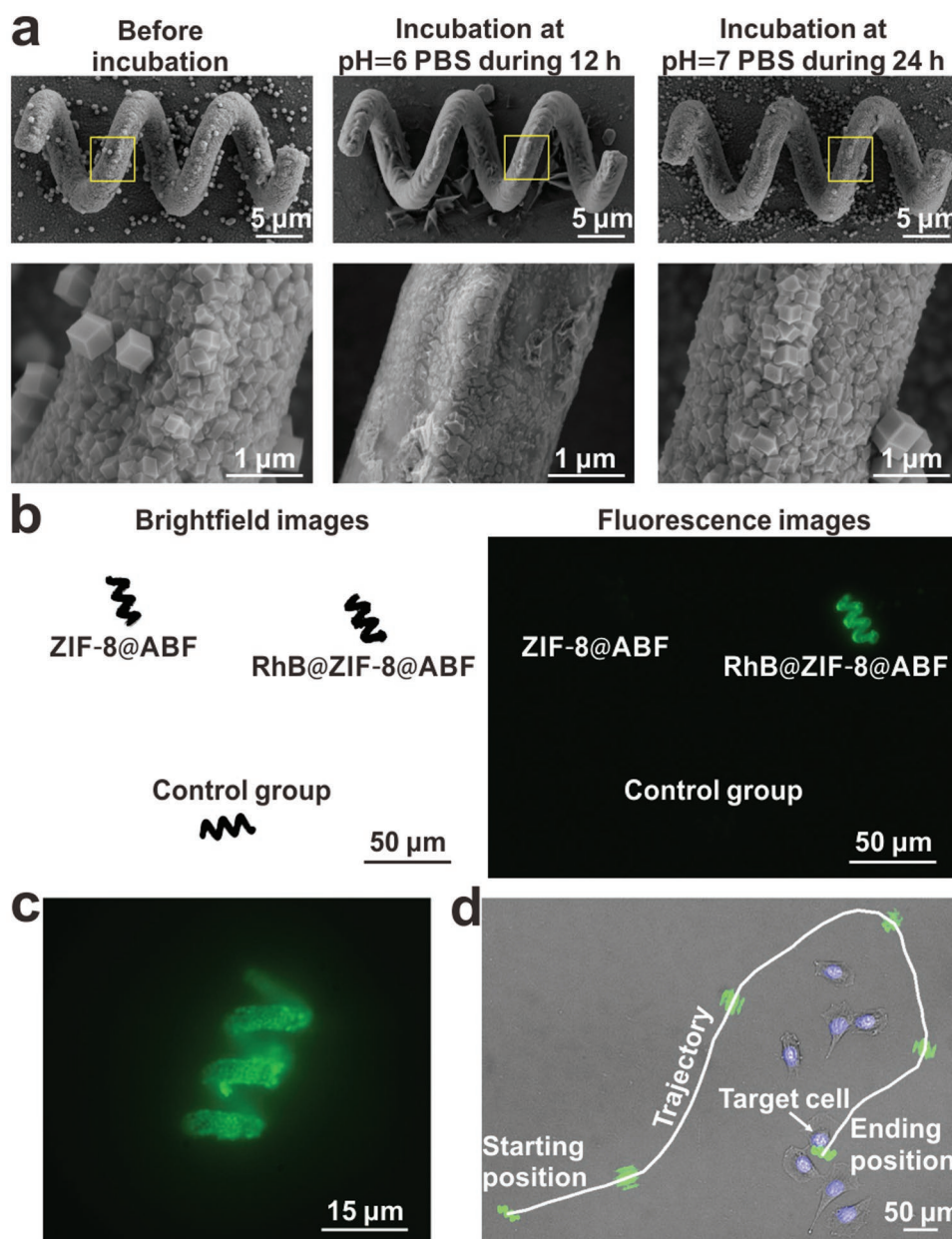
**ADVANCED
MATERIALS**

www.advmat.de

Figure 3. a) From left to right, SEM images of ZIF-8@ABF before incubation, after 12 h incubation at pH 6.0, and after 24 h incubation at pH 7.0. The series of SEM images in the bottom row are magnifications of the SEM images presented in the top row. b) Bright field and fluorescence images of a ZIF-8@ABF, an RhB@ZIF-8@ABF, and a control sample (ABF). c) Magnified fluorescence image of an RhB@ZIF-8@ABF. d) Microscopy image showing the movement of an RhB@ZIF-8@ABF structure along a complex trajectory, targeting a single cell.

Figure 3b shows the bright field and fluorescence images of a ZIF-8@ABF, an RhB@ZIF-8@ABF, and a control sample. The control sample corresponds to an ABF incubated with a methanolic solution of RhB (1×10^{-3} M) for 24 h in the absence of ZIF-8 precursors. From the micrographs shown in Figure 3b,c, we can see that RhB is only loaded in RhB@ZIF-8@ABFs. Moreover, to demonstrate the targeted drug delivery capabilities of motile RhB@ZIF-8@ABFs in biologically relevant media, we show that these devices can supply therapeutic payloads to a target region within a cell culture. Figure 3d shows the fluorescent images of an RhB@ZIF-8@ABF which was maneuvered to a specific target

cell localized on the surface of a Petri dish (see also Video S3 in the Supporting Information). Note that the RhB@ZIF-8@ABF was navigated along a predesigned customized trajectory toward a single cell, without touching any adjacent cells.

Under acidic buffer conditions (i.e., PBS at pH 6.0), RhB was clearly transferred from RhB@ZIF-8@ABFs to breast cancer cells (MDA-MB231) located on the surface of a Petri dish. **Figure 4** shows the brightfield and fluorescence images of breast cancer cells after being incubated for 3 h with RhB@ZIF-8@ABFs at pH 7.4 and pH 6.0. The data confirms that when RhB@ZIF-8@ABFs are navigated through an acidic
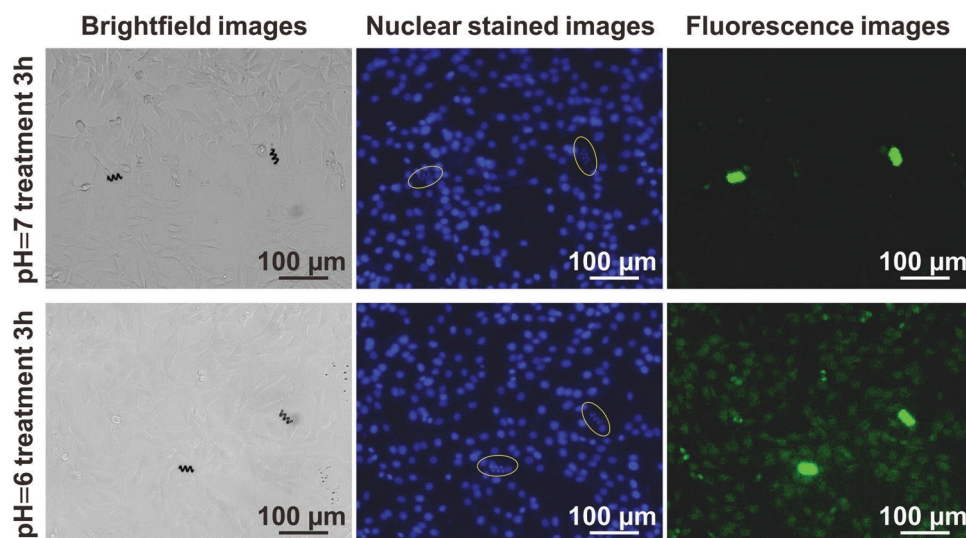
**ADVANCED
SCIENCE NEWS**

www.advancedsciencenews.com

**ADVANCED
MATERIALS**

www.advmat.de

Figure 4. In vitro model drug release of RhB@ZIF-8@ABF in PBS (pH 7.4) and PBS (pH 6.0) to fixed breast cancer cells (MDA-MB231).

environment, such as the extracellular medium of cancer tissues, the cargo loaded in ZIF-8@ABFs can be efficiently transferred to cells. The same swimmers navigated through a pH 7.4 environment remain intact, as confirmed by a lack of cellular emission throughout the field of view. In these experiments, breast cancer cell nuclei were stained with Hoechst 33342 to facilitate visualization of cell positions.

The controlled motion and drug delivery capabilities of these highly integrated multifunctional systems are further demonstrated within a complex microfluidic system incorporating pneumatic valves (**Figure 5**). This pneumatic microfluidic configuration allows for the controllable generation of two distinct microenvironments at pH 5.0 and 7.4 via pneumatic actuation

(Figure 5b). Four RhB@ZIF-8@ABFs were introduced at position 1 (P1) of the microfluidic device where the pH is 7.4. The ABFs were then maneuvered toward P4 trapping two ABFs at P4 (pH 5.0) and two ABFs at P2 (pH 7.4). This controlled positioning of the microrobots was achieved via pneumatic actuation of the integrated valves. As illustrated in Figure 5d, the RhB@ZIF-8@ABFs kept in P2 remain fluorescent, while the RhB@ZIF-8@ABFs located in P4 and P5 lose the fluorescence emission. This indicates that ZIF-8 degrades within a low pH environment, accompanied by cargo (RhB) discharge. Accordingly, this model experiment demonstrates that ZIF-8@ABFs are able to dispense drug-like molecules in a selective and controllable manner.
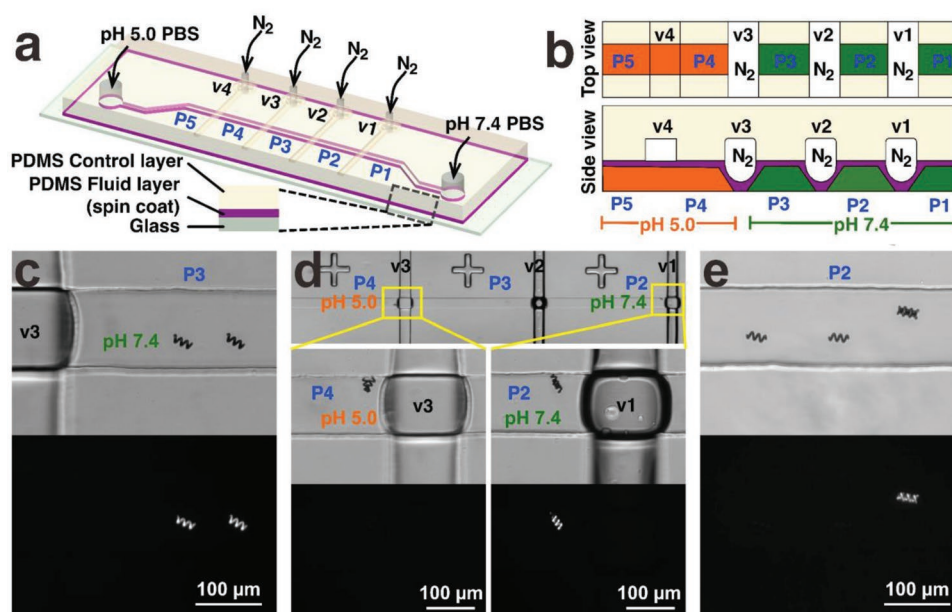

Figure 5. a) Schematic illustration of the microfluidic device used to demonstrate regioselective delivery of cargo. b) Side view of the microfluidic device, highlighting the pneumatic actuation of integrated valves. c–e) Series of brightfield and fluorescence microscopy images showing the control manipulation of RhB@ZIF-8@ABFs from P2 to P5 and back.

**ADVANCED
SCIENCE NEWS**

www.advancedsciencenews.com

**ADVANCED
MATERIALS**

www.advmat.de

In summary, we successfully developed an MOF-based ABF. These ABFs can be successfully maneuvered and controlled by magnetic microhelices with a corkscrew locomotion mechanism using only weak external magnetic fields. The MOF-based swimmers consist of a magnetically coated 3D printed helical framework, whose surface is coated with a highly biocompatible and pH-responsive Zn-based MOF (ZIF-8) surface coating. The thickness and compactness of the ZIF-8 coatings on the surface of such helical structures can be tailored by the variation of synthetic conditions (reactants concentration and reaction time). To illustrate the potential of the proposed MOF-based microrobots, we have shown that these swimmers can act as pH-responsive targeted drug delivery platforms, and they are able to carry and release drugs in biologically relevant environments similar to those encountered in the extracellular media of a tumor. We have also demonstrated that the proposed MOF-based microrobots can follow complex trajectories within microfluidic channels to deliver drugs in a regioselective manner.

Experimental Section

Fabrication of ZIF-8@ABFs: The ABFs were fabricated using a 3D Direct Laser lithography (Nanoscribe GmbH). Briefly, photoresist IPL-780 (negative-tone photoresist) was spin-coated on a glass substrate. The helical structure was designed with SolidWorks and loaded in the Nanoscribe software. During the two-photon lithography process, the laser power used was 13 mW, and the scan speed was 50 mm s^{-1}. Finally, the array of helical structures were developed in IPA for 10 min, and then dried with a nitrogen gun. Based on previous investigations,[15] we chose as a prototypical swimmer a helix with three turns, a helical diameter of around 10 µm, a filament diameter of approximately 3 µm, and a helical angle around 70°. This design provided good swimming performance at low magnitude rotating magnetic fields. Additionally, our swimmers exhibited a corkscrew regime at relatively low frequencies (10 Hz). The framework was coated first with nickel (90 nm) and then titanium (9 nm) successively with an electron beam evaporator (Plassys-II MEB550SL). A homogeneous coating was achieved by applying a tilt of 15° and a rotating speed of 20 rpm at the sample stage. The coated framework was then exposed to a O$_2$ plasma for 90 s to clean and oxidize the surface. After construction, the oxidized ABFs were treated with dopamine hydrochloride (2.5 mg mL^{-1}) in tris-hydroxymethyl aminomethane (10 × 10^{-3} M) for 24 h to grow a polydopamine layer on the ABF surface. Two solutions of zinc nitrate hexahydrate (20 × 10^{-3} M/50 × 10^{-3} M/100 × 10^{-3} M) and 2-methylimidazole (40 × 10^{-3} M/100 × 10^{-3} M/200 × 10^{-3} M) were then prepared in methanol and an equal amount of each solution was mixed and stirred for 1 min at 500 rpm. PDA-coated ABFs were immersed into the resulting mixture for a specific period of time (2 or 24 h). Finally, the modified ABFs were washed with methanol and dried with nitrogen.

Characterization of ZIF-8 Coatings: SEM images were taken to characterize the surface morphology of ZIF-8@ABFs. In addition, an EDX analysis was performed to confirm the presence of Zn, N, and C elements in ZIF-8 crystals. The XRD measurements were obtained from ZIF-8 crystals grown on a polydopamine deposited silicon wafer. For the ZIF-8@ABF synthesis, prior to the polydopamine treatment, the silicon wafer was coated with IPL-780 (polymerized by exposure to an LOT-Oriel 500 W Hg UV-Source for 10 min), nickel (90 nm) and titanium (9 nm).

ZIF-8@ABF Locomotion: The swimming behavior of ZIF-8@ABFs was investigated using an electromagnetic control system consisting of three pairs of Helmholtz coils to generate a rotational magnetic field. A ZIF-8@ABF sample was immersed in deionized water in a sample holder with a piece of clean silicon wafer. The sample holder was then placed at the center of the Helmholtz setup to ensure a uniform magnetic field. A microprobe (T-4-22, GGB Industries, Inc., USA) was then used to release the ZIF-8@ABF and transport it onto the silicon wafer. A rotational

magnetic field of 4 mT was applied to manipulate the ZIF-8@ABF. Variations in the direction and the rotating frequency of the magnetic field were used to maneuver ZIF-8@ABF along predefined trajectories.

Stability of ZIF-8@ABF as a Function of pH: PBS pH = 7.4 (1×) was purchased from Thermo Fisher Scientific. The acidic PBS solution was obtained by adjusting the pH value of PBS from 7.4 to 6.0 using phosphoric acid. The PBS solution at pH 5.0 was also obtained using this method. SEM images were acquired after incubating ZIF-8@ABFs at pH 6.0 and pH 7.4 for a given time period.

Fabrication of RhB@ZIF-8@ABF: The fabrication of the ABFs was explained above. RhB was incorporated into the medium used to grow ZIF-8 crystals. RhB (5 mg) was dissolved in a methanol solution containing zinc nitrate hexahydrate (5 mL, 50 × 10^{-3} M). A solution of 2-methylimidazole (5 mL, 100 × 10^{-3} M) in methanol was then added in drops, and the mixture was stirred at 500 rpm for 1 min. The PDA treated ABFs were then immersed in the resulting mixture and left to stand for 24 h. Finally, the samples were washed with methanol and then dried with a nitrogen gun.

Drug Delivery within Cell Culture: 3T3 cells (American Type Culture Collection (ATCC)) were fixed in a Petri dish using 4% paraformaldehyde in PBS (pH 7.4) and washed with PBS (pH 7.4). The cell nuclei were stained using Hoechst 33 342 (Thermo Fisher Scientific), and all cells were kept in PBS at pH 7.4 prior to experimentation. An RhB@ZIF-8@ABF was transferred to the Petri dish using a microprobe (T-4-22, GGB Industries, Inc., USA). A customized magnetic actuation system (MFG-100-I, MagnetbotiX AG, Switzerland) was used to generate rotational magnetic fields to manipulate the RhB@ZIF-8@ABF to a target region in the cell culture, following a predefined trajectory. Videos and images were taken with a fluorescence inverted optical microscope (Olympus IX-81, Olympus Optical Co. Ltd., Japan).

Drug Release Experiments: Breast cancer cells (MDA-MB231) (ATCC) were fixed in a Petri dish using 4% paraformaldehyde in PBS (pH 7.4) and washed with PBS (pH 7.4). Cell nuclei were stained using Hoechst 33342 (Thermo Fisher Scientific), and all cells were kept in PBS at pH 7.4 prior to experimentation. Two different solutions for cargo release were assessed, PBS pH 6.0 and PBS pH 7.4. After incubating the RhB@ZIF-8@ABF for 3 h, brightfield and fluorescence images were taken. A blue filter was used to extract fluorescence signals from cell nuclei and RhB, while a green filter was used to extract the fluorescence signal from RhB only.

Microfluidic Device Fabrication: Double layer, polydimethylsiloxane (PDMS) microfluidic devices were fabricated on silicon wafers (Okmetic, Finland) using conventional soft lithography techniques.[16] The top (control) layer was fabricated using replica molding.[17] First, a mixture of PDMS elastomer and curing agent (Sylgard 184, Dow Corning, Midland, USA) was prepared at a ratio of 5:1 w/w. This mixture was then put under vacuum for 30 min to remove trapped gases. The PDMS mixture was then poured on top of the silicon wafer containing the features for the "control layer" and the entire assembly cured at 70 °C for 30 min. To make the bottom (fluidic) layer, a degassed mixture of PDMS and curing agent (20:1 in weight) was spin-coated on the fluidic master mold in two consecutive steps (first 500 rpm for 10 s, and then 1200 rpm for 50 s). After spinning, the "fluidic" master mold was cured at 70 °C for a period of 15 min. The control layer was diced using a razor blade, and holes were formed using a Gauge 22 puncher (Technical Innovations Inc., Texas). The control layer was then assembled on top of the cured fluidic layer in the "fluidic" master mold. The two layers were placed in an oven at 70 °C overnight to ensure complete thermal bonding. Following this, the two bonded layers were removed from the "fluidic" master mold, diced with a razor blade, and 1.5 mm holes were formed using a biopsy punch (Miltex GmbH, Rietheim–Weilheim, Germany) in the fluidic layer. Finally, the double layer PDMS devices were bonded to a glass coverslip (24 mm x 60 mm, Menzel Glasbearbeitungswerk GmbH & Co. KG, Germany) using oxygen plasma activation.

Loading of RhB@ZIF-8@ABFs and Preparation of the Microfluidic Environment: The microfluidic device was designed with five regions that can be separated by pneumatic actuation of the integrated valves. Each valve consists of a thin PDMS membrane that can be deflected toward the glass substrate when nitrogen is pumped through the top (control) microfluidic layer. In the experiment, RhB@ZIF-8@ABFs were dispensed inside the microfluidic device (P1) through the inlet near P1. Note that

valve 1 (V1) was kept closed during the injection of the microrobots to prevent access to the microchamber P2. The RhB@ZIF-8@ABFs were dispensed with ethanol which evaporated after a few hours. A PBS solution (pH 7.4) was introduced in P1, when V1 and V2 were open and V3 was closed. At the same time, a PBS solution (pH 5.0) was injected through the inlet near P5, while V4 was open and V3 was closed. In this way, two well-defined microenvironments at different pH were generated.

Supporting Information

Supporting Information is available from the Wiley Online Library or from the author.

Conflict of Interest

The authors declare no conflict of interest.

[1] a) B. J. Nelson, I. K. Kaliakatsos, J. J. Abbott, *Annu. Rev. Biomed. Eng.* **2010**, *12*, 55; b) J. Wang, W. Gao, *ACS Nano* **2012**, *6*, 5745; c) X. Wang, C. Hu, L. Schurz, C. De Marco, X. Chen, S. Pané, B. J. Nelson, *ACS Nano* **2018**, *12*, 6210; d) X. Wang, X. H. Qin, C. Hu, A. Terzopoulou, X. Z. Chen, T. Y. Huang, K. Maniura-Weber, S. Pané, B. J. Nelson, *Adv. Funct. Mater.* **2018**, *28*, 1804107; e) D. Ahmed, T. Baasch, B. Jang, S. Pane, J. r. Dual, B. J. Nelson, *Nano Lett.* **2016**, *16*, 4968; f) X.-Z. Chen, N. Shamsudhin, M. Hoop, R. Pieters, E. Siringil, M. S. Sakar, B. J. Nelson, S. Pané, *Mater. Horiz.* **2016**, *3*, 113; g) D. Ahmed, C. Dillinger, A. Hong, B. J. Nelson, *Adv. Mater. Technol.* **2017**, *2*, 1700050; h) J. Li, B. E.-F. de Ávila, W. Gao, L. Zhang, J. Wang, *Sci. Rob.* **2017**, *2*, eaam6431; i) S. C. Lenaghan, Y. Wang, N. Xi, T. Fukuda, T. Tarn, W. R. Hamel, M. Zhang, *IEEE Trans. Biomed. Eng.* **2013**, *60*, 667; j) H. M. Li, J. D. Tan, M. J. Zhang, *IEEE Trans. Autom. Sci. Eng.* **2009**, *6*, 220; k) C. Bi, M. Guix, B. V. Johnson, W. Jing, D. J. Cappelleri, *Micromachines* **2018**, *9*, 68; l) L. O. Mair, S. Chowdhury, G. A. Paredes-Juarez, M. Guix, C. Bi, B. Johnson, B. W. English, S. Jafari, J. Baker-McKee, J. Watson-Daniels, O. Hale, P. Stepanov, D. Sun, Z. Baker, C. Ropp, S. B. Raval, D. R. Arifin, J. W. M. Bulte, I. N. Weinberg, B. A. Evans, D. J. Cappelleri, *Micromachines* **2019**, *10*, 230; m) W. Hu, K. S. Ishii, Q. Fan, A. T. Ohta, *Lab Chip* **2012**, *12*, 3821.

[2] a) G. Chatzipirpiridis, O. Ergeneman, J. Pokki, F. Ullrich, S. Fusco, J. A. Ortega, K. M. Sivaraman, B. J. Nelson, S. Pané, *Adv. Healthcare Mater.* **2015**, *4*, 209; b) F. Qiu, S. Fujita, R. Mhanna, L. Zhang, B. R. Simona, B. J. Nelson, *Adv. Funct. Mater.* **2015**, *25*, 1666; c) M. Sitti, H. Ceylan, W. Hu, J. Giltinan, M. Turan, S. Yim, E. Diller, *Proc. IEEE* **2015**, *103*, 205.

[3] H.-W. Huang, M. S. Sakar, A. J. Petruska, S. Pané, B. J. Nelson, *Nat. Commun.* **2016**, *7*, 12263.

[4] a) Y. Ikezoe, G. Washino, T. Uemura, S. Kitagawa, H. Matsui, *Nat. Mater.* **2012**, *11*, 1081; b) B. Khezri, M. Pumera, *Adv. Mater.* **2019**, e1806530.

[5] A. Ayala, C. Carbonell, I. Imaz, D. Maspoch, *Chem. Commun.* **2016**, *52*, 5096.

[6] J. Li, X. Yu, M. Xu, W. Liu, E. Sandraz, H. Lan, J. Wang, S. M. Cohen, *J. Am. Chem. Soc.* **2017**, *139*, 611.

[7] a) S. K. Elsaidi, M. A. Sinnwell, A. Banerjee, A. Devaraj, R. K. Kukkadapu, T. C. Droubay, Z. Nie, L. Kovarik, M. Vijayakumar, S. Manandhar, *Nano Lett.* **2017**, *17*, 6968; b) G. Lu, S. Li, Z. Guo, O. K. Farha, B. G. Hauser, X. Qi, Y. Wang, X. Wang, S. Han, X. Liu, *Nat. Chem.* **2012**, *4*, 310; c) P. Falcaro, F. Normandin, M. Takahashi, P. Scopece, H. Amenitsch, S. Costacurta, C. M. Doherty, J. S. Laird, M. D. Lay, F. Lisi, *Adv. Mater.* **2011**, *23*, 3901; d) P. Falcaro, F. Lapierre, B. Marmiroli, M. Styles, Y. Zhu, M. Takahashi, A. J. Hill, C. M. Doherty, *J. Mater. Chem. C* **2013**, *1*, 42.

[8] a) C. Y. Sun, C. Qin, X. L. Wang, G. S. Yang, K. Z. Shao, Y. Q. Lan, Z. M. Su, P. Huang, C. G. Wang, E. B. Wang, *Dalton Trans.* **2012**, *41*, 6906; b) H. Ren, L. Zhang, J. An, T. Wang, L. Li, X. Si, L. He, X. Wu, C. Wang, Z. Su, *Chem. Commun.* **2014**, *50*, 1000; c) H. Q. Zheng, Y. N. Zhang, L. F. Liu, W. Wan, P. Guo, A. M. Nystrom, X. D. Zou, *J. Am. Chem. Soc.* **2016**, *138*, 962.

[9] Y. Wang, K. Zhou, G. Huang, C. Hensley, X. Huang, X. Ma, T. Zhao, B. D. Sumer, R. J. DeBerardinis, J. Gao, *Nat. Mater.* **2014**, *13*, 204.

[10] a) R. Mhanna, F. Qiu, L. Zhang, Y. Ding, K. Sugihara, M. Zenobi-Wong, B. J. Nelson, *Small* **2014**, *10*, 1953; b) W. Cai, J. Wang, C. Chu, W. Chen, C. Wu, G. Liu, *Adv. Sci.* **2019**, *6*, 1801526; c) P. Erkoc, I. C. Yasa, H. Ceylan, O. Yasa, Y. Alapan, M. Sitti, *Adv. Ther.* **2019**, *2*, 1800064.

[11] a) Q. Ye, F. Zhou, W. Liu, *Chem. Soc. Rev.* **2011**, *40*, 4244; b) Q. Liu, N. Wang, J. Caro, A. Huang, *J. Am. Chem. Soc.* **2013**, *135*, 17679; c) J. Zhou, P. Wang, C. Wang, Y. T. Goh, Z. Fang, P. B. Messersmith, H. Duan, *ACS Nano* **2015**, *9*, 6951.

[12] A. J. Howarth, Y. Liu, P. Li, Z. Li, T. C. Wang, J. T. Hupp, O. K. Farha, *Nat. Rev. Mater.* **2016**, *1*, 15018.

[13] D. Fairen-Jimenez, S. Moggach, M. Wharmby, P. Wright, S. Parsons, T. Duren, *J. Am. Chem. Soc.* **2011**, *133*, 8900.

[14] a) S. Fusco, G. Chatzipirpiridis, K. M. Sivaraman, O. Ergeneman, B. J. Nelson, S. Pane, *Adv. Healthcare Mater.* **2013**, *2*, 1037; b) H. Li, G. Go, S. Y. Ko, J. O. Park, S. Park, *Smart Mater. Struct.* **2016**, *25*, 027001; c) J. X. Li, S. Thamphiwatana, W. J. Liu, B. E. F. de Avila, P. Angsantikul, E. Sandraz, J. X. Wang, T. L. Xu, F. Soto, V. Ramez, X. L. Wang, W. W. Gao, L. F. Zhang, J. Wang, *ACS Nano* **2016**, *10*, 9536.

[15] S. Tottori, L. Zhang, F. Qiu, K. K. Krawczyk, A. Franco-Obregon, B. J. Nelson, *Adv. Mater.* **2012**, *24*, 811.

[16] B. Z. Cvetkovic, J. Puigmarti-Luis, D. Schaffhauser, T. Ryll, S. Schmid, P. S. Dittrich, *ACS Nano* **2012**, *7*, 183.

[17] Y. Xia, G. M. Whitesides, *Annu. Rev. Mater. Sci.* **1998**, *28*, 153.